Solar Energy 221 (2021) 488–501

Contents lists available at ScienceDirect

Solar Energy

journal homepage: www.elsevier.com/locate/solener

Design of a highly efficient CdTe-based dual-heterojunction solar cell with 44% predicted efficiency

Abdul Kuddus [a,b], Abu Bakar Md. Ismail [a], Jaker Hossain [a,*]

[a] Solar Energy Laboratory, Department of Electrical and Electronic Engineering, University of Rajshahi, Rajshahi 6205, Bangladesh
[b] Graduate School of Science and Engineering, Saitama University, Saitama 338-8570, Japan

ARTICLE INFO

Keywords:
CdS/CdTe solar cells
ITO TCO
CdSe and Sb_2Se_3 BSF
Photovoltaics
SCAPS-1D simulation

ABSTRACT

In this article, we theoretically demonstrate highly efficient cadmium telluride (CdTe)-based dual-heterojunction solar cells (DHSCs) with incorporating cadmium selenide (CdSe) and antimony selenide (Sb_2Se_3), separately as back surface field (BSF) layer using SCAPS-1D simulator. The impacts of various physical parameters have been investigated in details on the photovoltaic performance of the designed cells. It is found that the power conversion efficiency (PCE) of the pristine CdTe solar cell significantly increases by the use of CdSe and Sb_2Se_3 BSF layers. The optimized PCE of the CdTe solar cell increases from 21.29% for pristine SC to 31.11% with Voc = 1.15 V, Jsc = 30.66 mA/cm^2 and FF = 88.57% owing to the use of CdSe BSF layer. On the other hand, the PCE of CdTe DH solar cell enhances to 44.14% with Voc = 1.05 V, Jsc = 49.23 mA/cm^2 and FF = 85.71%, respectively by the use of Sb_2Se_3 BSF layer which is almost consistent with the detailed-balance limit of DHSC. These findings reveal that both the CdSe and Sb_2Se_3 could be promising BSFs for the fabrication of cost effective, highly efficient CdTe-based dual-heterojunction solar cells.

1. Introduction

The global energy crisis and green-house effect are the serious issues that have compelled the researchers to study the renewable energy technology and over the last few decades, there has been a significant progress on the renewable energy research, especially in the field of solar photovoltaics (PV). Various types of solar cells such as silicon, Cadmium Telluride (CdTe), copper indium gallium arsenide (CIGS) and III-V compound-semiconductor-based solar cells have intensively been studied to fabricate highly efficient solar cell. Among these solar cells including perovskites have been studied intensively to fabricate highly efficient solar cells (Bhattacharya and John, 2019; Zhang et al., 2021; Enkhardt, 2020; Gao et al., 2020; Wang et al., 2020a; Wang et al., 2020b). In recent times, perovskites solar cells comprising the interface modification together with stability offer the cell efficiency of $\geq$ 20% with enhanced stability (M. Wang et al., 2020; Hu et al., 2020). Moreover, wafer-based first-generation (1G) silicon solar cell possesses over 90% of the global PV market as it is stable, non-toxic, abundant and well understood material (Andreani et al., 2019; Battaglia et al., 2016; Hossain, J., et al., 2021). Recently, an efficiency (η) of 26.33% with a practical module size of 180 cm^2 in back contact structure has been reported for the silicon solar cells (Yoshikawa et al., 2017). However, silicon is an indirect band gap material with relatively weak light absorption coefficient and it requires extremely high temperature of ~1400 °C for the processing of silicon solar cells (Andreani et al., 2019).

Moreover, the second-generation (2G) thin film solar cell structure based on CdTe and CIGS shows a good absorption coefficient at visible spectrum range and give a modest power conversion efficiency, but still their efficiency is not comparable to that of silicon solar cells and manufacturing costs progressively dominates by the constituent materials, such as, the top cover sheet and other encapsulants (Moon et al., 2020; Green, 2001). Although, thermodynamics exhibits that 93% of sunlight can be converted to electricity using an infinite number of stacked multi-junction solar cells as opposed to the upper limit on the conversion efficiency of 33% of a single junction solar cell, as is the scenario of the silicon wafer as well as most of the current thin film devices (Green, 2020). In addition, the detailed balance limit of efficiency of a dual-heterojunction solar cell is about 42% that only considers the band bap of different layers (De Vos, 1980). It does not consider other factors such as conduction and valance band offsets, doping concentration of the constituent materials of the solar cell. This indicates that the performance of solar cells can be enhanced2-3 times

* Corresponding author.
E-mail address: jak_apee@ru.ac.bd (J. Hossain).

https://doi.org/10.1016/j.solener.2021.04.062
Received 18 November 2020; Received in revised form 11 April 2021; Accepted 30 April 2021
Available online 11 May 2021

by introducing different fundamentals concepts in their design to fabricate a third-generation (3G) high performance and low-cost solar cell (Moon et al., 2020; Green, 2020; De Vos, 1980).

Although, compound-semiconductor-based four-junction GaInP/GaAs/GaInAs/GaInAs solar cell shows a high η of 44.7%, but it requires highly expensive and sophisticated deposition techniques like molecular beam epitaxy (MBE) and molecular organic chemical vapor deposition (MOCVD) that significantly increases the device cost (Dimroth, 2014). Therefore, a different device concept is indispensable that fundamentally will enhance the cell efficiency with cost effective fabrication technique of cells.

In this article, we unveil a high efficiency CdTe-based dual- heterojunction solar cell by simulation approach to meet the criteria of 3G solar cells design using SCAPS (Solar Cell Capacitance Simulator)-1D simulator. SCAPS-1D simulator employing drift–diffusion method essentially operates based on the mathematical solution of Poisson's equation and the continuity equations for free electrons and free holes (Biplab et al., 2020; Ahmmed et al., 2020b). Therefore, it can take into account the effect of band offset, carrier mobility, doping concentration and the band gap.

Recently, CdTe has been proven to be one of the most leading thin film absorber materials for the applications in solar cell. Photoconversion efficiency $\geq$ 21.0% with an open-circuit voltage >1 V have observed for this solar cell in recent time (Moon et al., 2021; Clover Ian, 2015; Green et al., 2020; Burst et al., 2016). Today, CdTe based solar cells have achieved the global PV market with a market share of ~ 5.1%, specifically for thin film solar cells, and it is considered as the second cost-effective material after silicon (Razykov et al., 2011). Recently, CdTe solar cell module has been reported to have 18% efficiency with use of $Mg_xZn_{1-x}O$ (MZO) as window layer instead of CdS (Munshi et al., 2018). And also, it has been predicted that the efficiency of the CdTe based solar cells can be further enhanced to 28.04% using NiO hole transport layer (Ahmmed et al., 2020b).

Herein, we introduce the highly conductive CdSe and Sb_2Se_3 thin film separately as BSF layerfor the efficiency enhancement of the CdS/CdTe heterojunction solar cells. CdSe is an n-type II-VI semiconductor with a direct band gap of 1.7 eV (Baines et al., 2018). It is widely used in light emitting diodes, solar cells as well as photoelectrochemical cells (Baines et al., 2018; Li et al., 2018). Various techniques including Electrodeposition (Shenouda and El Sayed, 2015), chemical bath deposition (CBD) (Chate et al., 2012), pulsed laser deposition (PLD) (Bao et al., 2016; Yang et al., 2016), thermal evaporation (Lakshmi Shree et al., 2016), spray pyrolysis (Yadav et al., 2010) and radio frequency magnetron sputtering (Paudel and Yan, 2014), etc. have been employed to deposit CdSe thin films. P-type CdSe can be synthesised by molecular beam epitaxy using a nitrogen plasma source (Ohtsuka et al., 1994), with addition of p-type dopant such as Li, Na, and P to deposit bulk p-CdSe crystals with hexagonal structure (Henry et al., 1971). So far, CdSe has mainly been used as a window layer as a replacement of CdS in CdTe solar cells (Baines et al., 2018). On the other hand, solution processed p or n- CdSe may offers the easiest and cost effective way to fabricate high efficiency CdTe based photovoltaics (Bayramoglu et al., 2017; Najim et al., 2018; Baines et al., 2018). However, there is hardly any report of highly doped p-type CdSe as BSF layer in CdTe solar cells.

On the other hand, Antimony selenide (Sb_2Se_3) is a p-type inorganic semiconductor with an orthorhombic phase (Liu et al., 2019). It has an in direct band gap in the range of 1.0–1.5 eV (Chen et al., 2015; Kosek et al., 1978; Mueller and Wood, 1972; El-Shair et al., 1991; Černošková et al., 2014; El-Sayad, 2008; Birkett et al., 2018) and direct band gap in the range of 1.2 to 1.9 eV (Chen et al., 2015; El-Shair et al., 1991) depending on the deposition methods and treatment conditions. It has a hole mobility up to 42 $cm^2.V^{-1}.s^{-1}$ and high absorption coefficient ($>10^5$ cm^{-1}) (Z. Q. Li et al., 2019). These physical parameters have made Sb_2Se_3 is a suitable absorber material for the applications in photovoltaics. The p-type carrier concentration of Sb_2Se_3 can be increased by doping with S, Sn, and Cu etc. (El-Sayad, 2008; Chen et al., 2018; Ren et al., 2020). The highest efficiency of fabricated solar cells with Sb_2Se_3 as absorber layer shows the efficiency of 9.2% (Li et al., 2019). However, there are very few reports on the use of Sb_2Se_3 material as a BSF layer.

Table 1
Simulation parameters used for the n-CdS/p-CdTe/ p^+-CdSe or p^+-Sb_2Se_3 dual-heterojunction solar cells at 300 K.

Parameters	ITO	n-CdS	p-CdTe	CdSe	Sb_2Se_3
Thickness (nm)	50	100*	1500*	100*	100*
Band gap (eV)	3.60	2.42	1.50	1.7	1.53
Electron affinity (eV)	4.5	4.30	4.28	3.93	4.04
Dielectric permittivity (relative)	8.90	9.35	10.30	9.50	18.00
CB effective density of states ($1/cm^3$)	2.20×10^{18}	2.20×10^{18}	9.20×10^{17}	2.80×10^{19}	2.20×10^{18}
VB effective density of states ($1/cm^3$)	1.800×10^{19}	1.800×10^{19}	5.20×10^{18}	1.20×10^{19}	1.80×10^{19}
Electron thermal velocity (cm/s)	1.00×10^7	1.00×10^7	1.00×10^7	1.00×10^7	1.00×10^7
Hole thermal velocity (cm/s)	1.00×10^7	1.00×10^7	1.00×10^7	1.00×10^7	1.00×10^7
Electron mobility (cm^2/Vs)	5.00×10^1	1.00×10^2	3.20×10^2	0.593×10^1	1.50×10^1
Hole mobility (cm^2/Vs)	1.00×10^1	2.50×10^1	4.00×10^1	2.50×10^1	5.10×10^0
Shallow uniform donor density, N_D ($1/cm^3$)	1.00×10^{21}	1.15×10^{17}*	1.00×10^7	1.00×10^7	1.00×10^7
Shallow uniform acceptor density, N_A ($1/cm^3$)	1.00×10^7	1.00×10^7	1.00×10^{16}*	1.00×10^{19}*	1.00×10^{19}*
Radiative recombination coefficient (cm3/s)	2.3×10^{-11}	2.3×10^{-9}	2.3×10^{-9}	2.3×10^{-9}	2.3×10^{-9}
Defect density (cm^{-3}) (above E_vw.r.t.E_{ref} (eV))	0.60	0.60	0.60	0.60	0.60
	1.00×10^{10}	1.00×10^{16}	1.00×10^{16}	1.00×10^{16}	1.00×10^{16}
Resistances	Series = 0–11 Ω cm^2 and Shunt 1.5–0.1 K Ω-cm^2				
Interface defect parameters used in the device simulation					
Parameters	CdS/CdTe interface			CdTe/ CdSe or Sb_2Se_3 interface	
Defect type	Neutral			Neutral	
Capture cross section electrons (cm^2)	1×10^{-19}			1×10^{-19}	
Capture cross-section holes (cm^2)	1×10^{-19}			1×10^{-19}	
Reference for defect energy level E_t	Above highest E_v			Above highest E_v	
Energy with respect to Ref. (eV)	0.250			0.250	
Total density (cm^{-2})	1.0×10^{14}			1.0×10^{14}	

"*"indicates a variable parameters.

In this article, we theoretically demonstrate the effect of different physical parameters of CdS, CdTe, CdSe and Sb_2Se_3 layers on the photovoltaic parameters of the designed ITO/CdS/CdTe/CdSe (or Sb_2Se_3) solar cells. This study reveals that the incorporation of highly degenerate CdSe and Sb_2Se_3BSF layers are promising for the high efficiency CdS/CdTe dual-heterojunction solar cells.

2. Device modeling and simulation

The CdS/CdTe heterojunction solar cells were simulated using SCAPS-1D simulation software considering the significant conditions and variables as reported elsewhere (Ahmmed et al., 2020b; Burgelman et al., 2004; Simya et al., 2015; Movla, 2014; Kuddus et al., 2019). One sun illumination (100 mW cm^{-2}) and global air mass (AM) 1.5 spectrum at temperature of 300 Kwere used to simulate the designed solar cell structure where ideal values for series (Rs) and Shunt (Rsh) resistance were set. In this simulation, ITO and Mo were used as front and rear contacts.

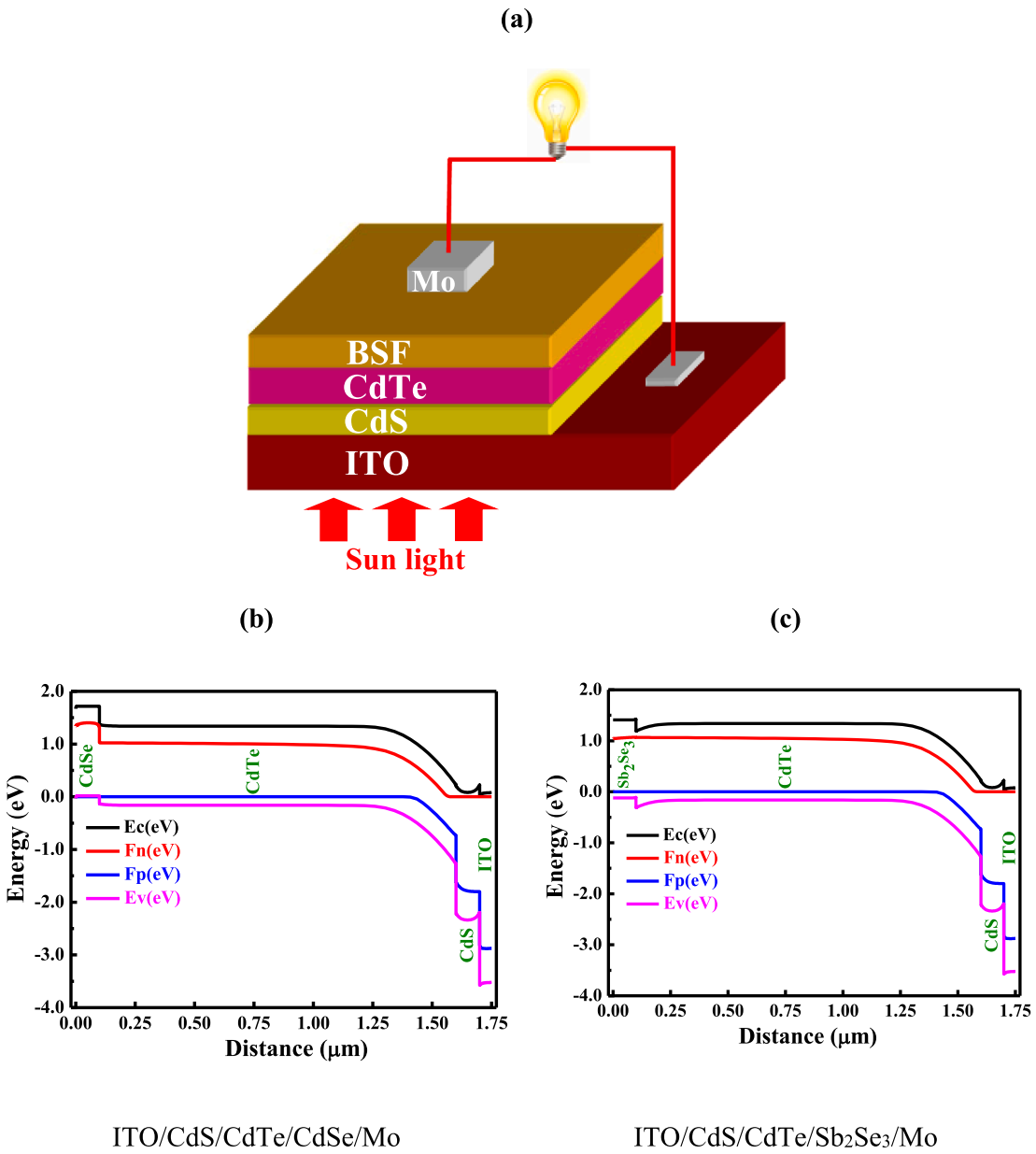

Fig. 1. The (a) schematic structure and energy band diagram with (b) CdSe and (c) Sb_2Se_3 BSF layer, respectively of CdTe-based dual-heterojunction solar cells.

The optical band gap, carrier concentration and other parameters employed in the solar cell structure simulation were collected from the experimental data and other research works (El-Shair et al., 1991; absorption coefficient, PV Education, 2020; Khudiar et al., 2012; Suzuki, H., 1966; Kuddus et al., 2020; Rahman et al., 2020b; Rahman et al., 2020a; Ahmmed et al., 2020a). The parameters used in this simulation for the characterization of CdS/CdTe solar cell structure are shown in Table 1. It can also be seen from the table that the significant amount of bulk and interface defects have considered in the simulation to have the realistic solar cell devices in practice.

3. Results and discussion

3.1. CdS/CdTe solar cells with and without BSF layer

Fig. 1(a), b and c delineate the schematic structure and energy band diagram of CdS/CdTe heterojunction solar cell with CdSe and Sb_2Se_3 BSF layer, respectively. The CdTe is a p-type semiconductor with a band gap of 1.5 eV. The E_C and E_V of this semiconductor are 4.28 and 5.78 eV, respectively. On the other hand, the band gap of CdS is 2.4 eV and E_C and E_V of this semiconductor are 4.30 and 6.7 eV, respectively. Therefore, CdTe forms a favourable pn junction with CdS.

On the other hand, electron affinity of CdSe is 3.93 eV (Suzuki, H., 1966) and band gap of this semiconductor is 1.7 eV. Therefore, this semiconductor also forms a suitable pp^+ heterojunction with CdTe thus acting as a BSF layer when heavily doped as shown in Fig. 1(b). The electron affinity of Sb_2Se_3 is 4.04 eV. The band gap of vacuum evaporated Sb_2Se_3 thin films annealed at 200 °C is about 1.53 eV (El-Shair et al., 1991). Therefore, Sb_2Se_3 layer also forms a suitable pp^+ heterojunction with CdTe and acts as a promising BSF layer when heavily doped as depicted in Fig. 1(c).

3.2. Impact of absorber and window layer on PV parameters of CdS/CdTe solar cell without BSF layer

3.2.1. Effect of absorber layer

The effects of CdTe absorber layer thickness, carrier concentration and defect concentration on the performance of CdS/CdTe solar cell

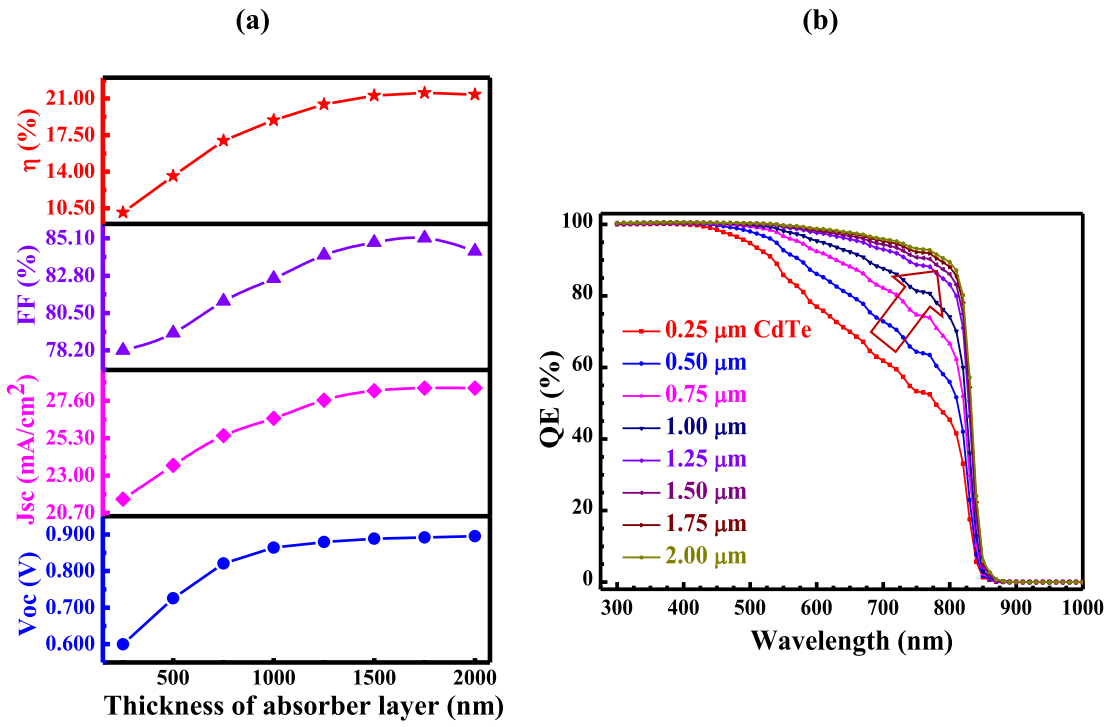

Fig. 2. The variation of (a) output parameters (Voc, Jsc, FF and η) and (b) corresponding quantum efficiency of CdS/CdTe solar cells with respect to the thickness of CdTe absorber layer.

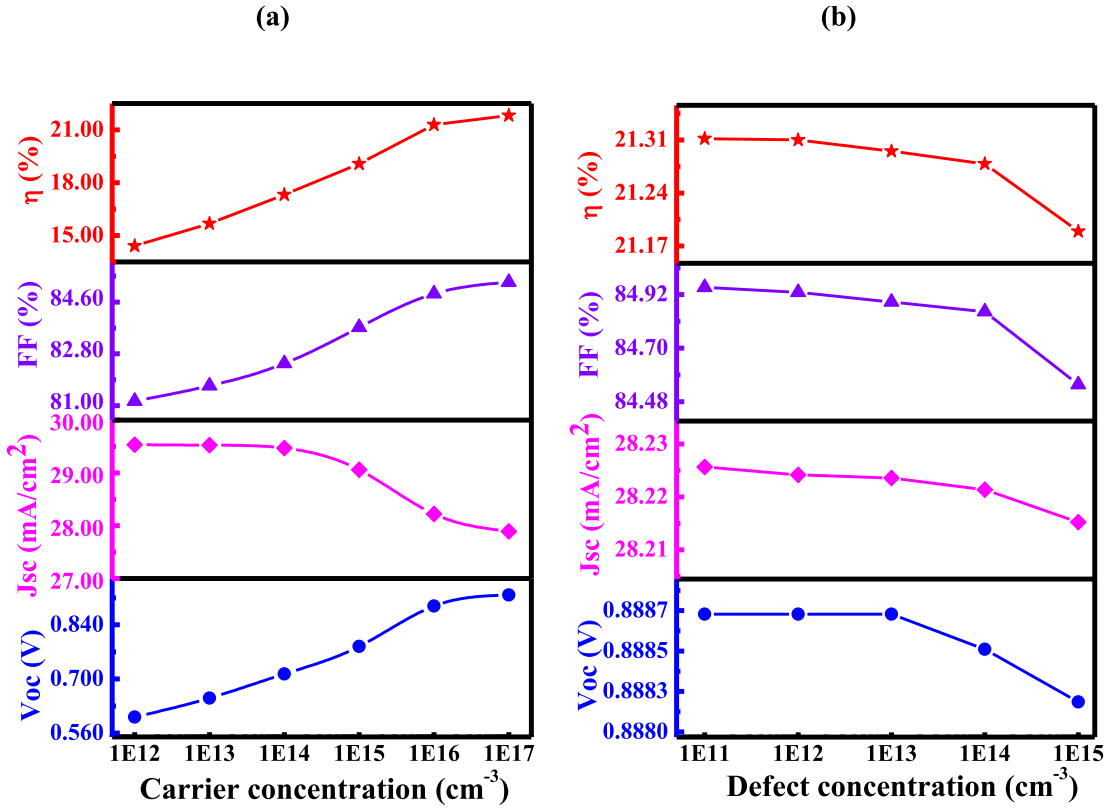

Fig. 3. The variation of output parameters (Voc, Jsc, FF and η) of CdS/CdTe solar cells with respect to (a) carrier concentration and (b) defect density of CdTe absorber layer.

have been discussed in this section. Fig. 2 demonstrates the photovoltaic performance of CdS/CdTe solar cell with respect to the thickness of CdTe absorber at constant carrier and defects densities of 10^{16} and 10^{14} cm^{-3}, respectively. In Fig. 2(a), it is clearly seen that the photovoltaic parameters: open circuit voltage (Voc), short circuit current (JSC) and fill factor increase with the increment of the absorber layer thickness up to

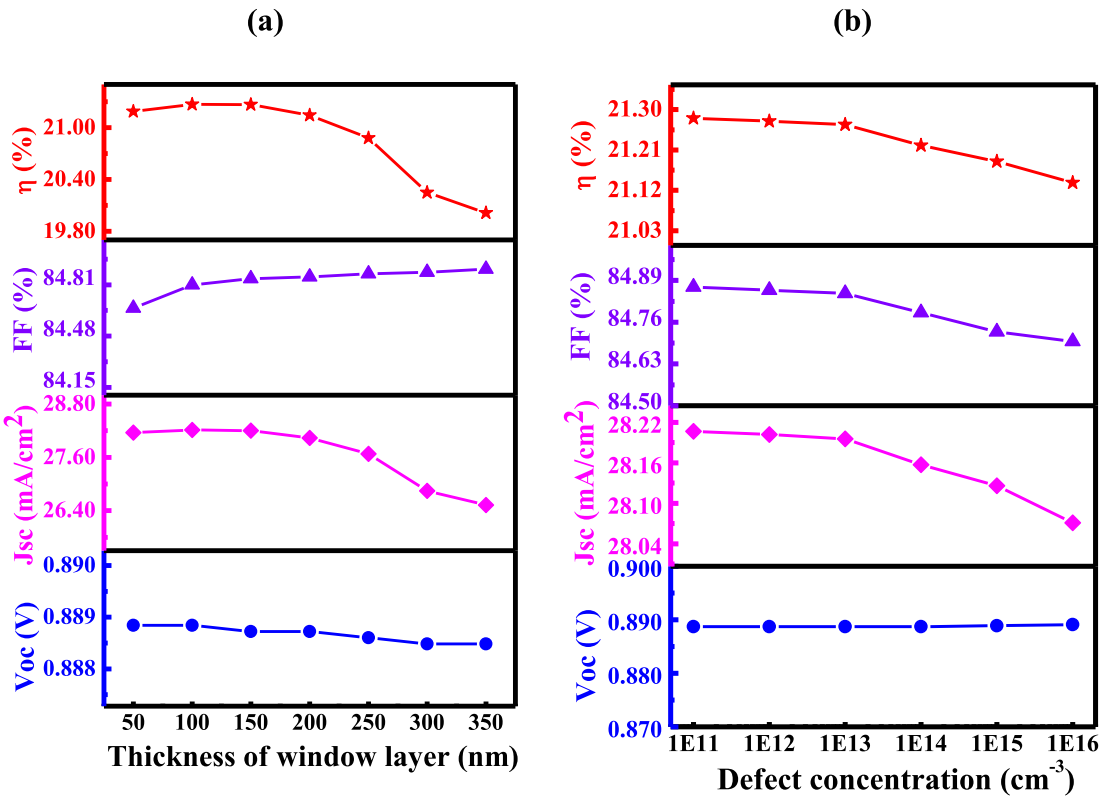

Fig. 4. The variation of output parameters (Voc, J_{SC}, FF and η) of CdS/CdTe solar cells with respect to (a) thickness and (b) defect density of CdS window layer.

1500 nm from 250 nm and consequently the photoconversion efficiency increases from ~ 9.5% to ~ 21.29%. Further increment of the absorber layer thickness beyond 1500 nm to 1700 nm, the cell parameters tends to remain constant at its highest value. The layer thickness of over 1700 nm, cell performance start to decrease noticeably due to apparent decrement of FF from 85.2 to 84.1% while Jsc decreases slightly from 28.4 to 28.25 mA/cm^2. The lower spectral absorption at thin CdTe is the reason of lower cell efficiency, but with the increases of the layer thickness, cell performance increases due to higher absorption of the spectral rays up to 1700 nm. The thick CdTe layer ($\lambda \geq 1500$ nm) enhances the recombination of the photogenerated carriers, therefore the photoconversion efficiency of the cell decreases. Fig. 2(b), curve of quantum efficiency (QE) with corresponding thickness reveals this similar consequence for the CdTe thickness of 250–2000 nm. Therefore, the CdTe layer thickness of ~ 1500 nm with η ~ 21% has been chosen for further investigation for the both CdSe and Sb_2Se_3 BSF layer.

Fig. 3(a) shows the effect of the carrier concentration of CdTe absorber layer in the range of 10^{12} to 10^{17} cm^{-3} to explore the cell performance with constant thickness of 1500 nm. It is clearly seen from the figure that with increment of the carrier concentration of the CdTe absorber, the Voc and FF and consequently the PCE of the CdS/CdTe cell increases up to ~ 22.5% and then tends to be constant where the Jsc decreases to a small extent. This is due to the increment of the recombination among the abundant carriers throughout the cell with the increase of carrier concentration above 10^{16} cm^{-3}. At higher carrier concentrations of the CdTe absorber layer, impurity scattering and carrier recombination rate increases. Therefore, the hole transportation is suppressed at the CdTe absorber layer to CdSe or Sb_2Se_3 BSF layer. Considering these effects, a marginal level of the carrier concentration of the CdTe absorber layer was considered and which was 10^{16} cm^{-3}. On other hand, the existence of dislocations and the grain boundaries collectively known as defects act as a carrier trapping center that reduces the carrier lifetime. So, the defect density is one of critical parameters for designing photovoltaic cell.

The cell performance was studied as a function of defect density of the CdTe absorber layer as shown in Fig. 3(b). It is observed that the cell performance changes slightly up to defect density of 10^{14} cm^{-3} of CdTe absorber and then, tends to falls down quickly with the increase of the defect density. At a higher defect density of CdTe, the recombination rate is modulated with the SRH recombination. This study conjectures that the SRH plays a huge impact on the reduction of cell efficiency for higher defect density (>10^{15} cm^{-3}) of CdTe absorber layer. From this study, an optimum PCE of ~ 21.29% was found at the CdTe carrier concentration of 10^{16} cm^{-3}, the thickness of ~ 1500 nm at defect density of 10^{14} cm^{-3}. These results are comparable as well as more promising than reported articles (Tinedert et al., 2020; Parashar et al., 2020).

3.2.2. *Effect of window layer*

Fig. 4(a) and b show the effect of thickness and defect concentration of CdS window layer on PV performances of CdS/CdTe solar cells, respectively. The thickness of CdS was varied from 50 to 350 nm. It is observed from the Fig. 4(a) that the Jsc reduces from ~ 28.3 to ~ 26.40 mA/cm^2 with increasing the window layer thickness from 50 to 350 nm. Due to increase of parasitic absorption with thickness of window CdS layer, the lower wavelength photons are perturbed to reach the absorber layer and consequently the output current is reduced. The overall PCE reduces from 21.29 to 20.1% with increasing window layer thickness from 50 to 350 nm. In this investigation, CdS window layer thickness of 100 nm was chosen for further study. Fig. 4(b) depicts that the V_{OC} of ~ 0.89 V is almost independent with the defect concentration of CdS window layer. The similar results for current and voltage for CdS/CdTe solar cell were also found in a recent report (Parashar et al., 2020). The J_{SC} and FF show the negligible reducing tends with increment of CdS defect density from 10^{11} to 10^{16} cm^{-3}. Since, the thickness of window layer comparatively smaller, significant number of carriers can escape the defect states. The similar effect is also observed in previously reported articles (Kuddus et al., 2020; Parashar et al., 2020). Therefore, it can be concluded that defect density of CdS window layer has negligible

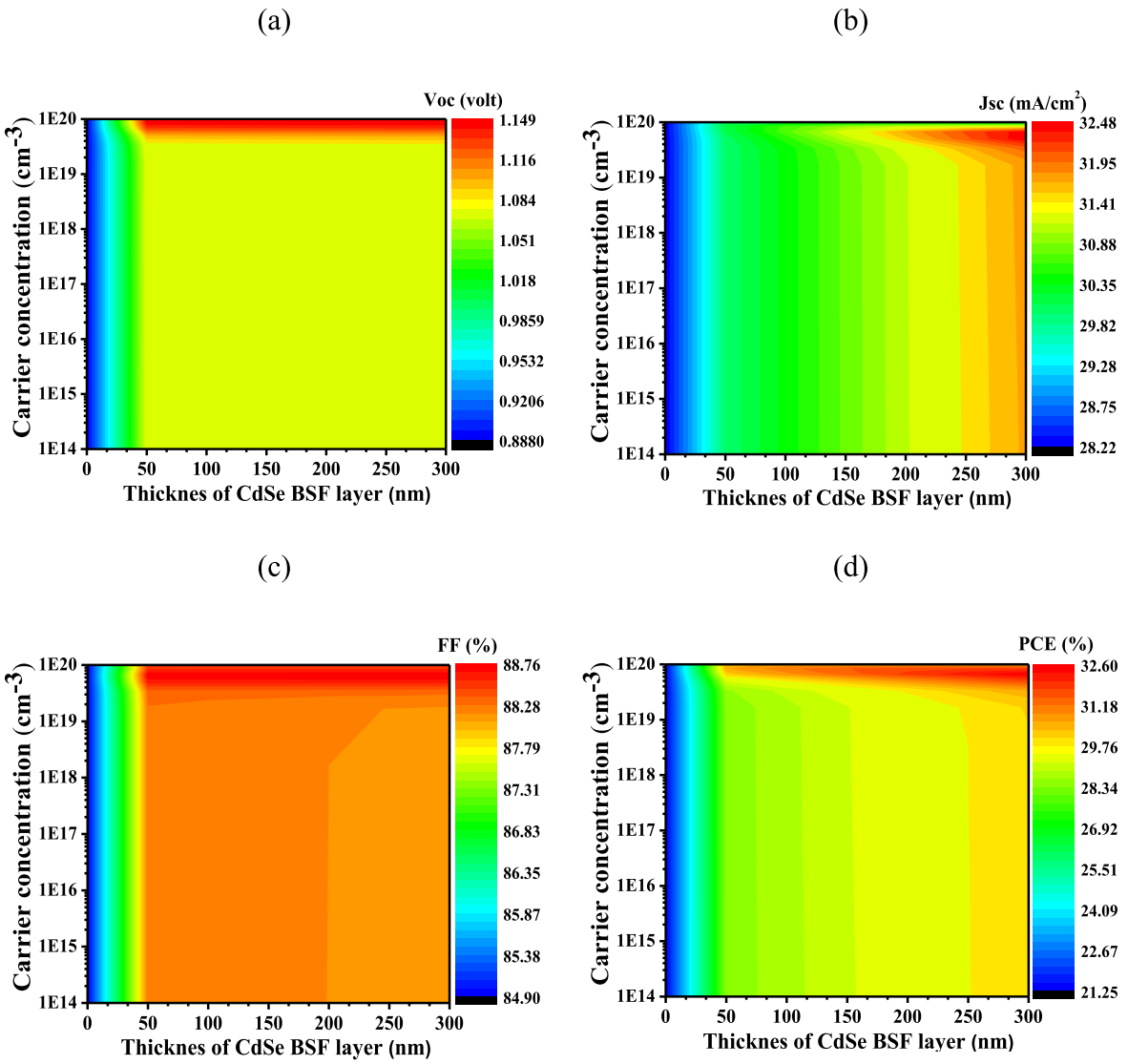

Fig. 5. The variation of output parameters (a) Voc, (b) Jsc (c) FF and (d) η of CdS/CdTe solar cells with respect to carrier concentration and thickness of CdSe BSF layer.

effects on photovoltaic parameters of CdS/CdTe-based heterojunction solar cells. For the superlative utilization of the higher wavelength rays of solar spectrum and therefore achieving remarkable improvement of the PCE of CdS/CdTe solar cell, further investigation with CdSe and Sb_2Se_3 BSF has been performed by the use of these optimized conditions for absorber and window layer of CdS/CdTe solar cell.

3.3. *Effect of CdSe BSF layer on PV performance of CdTe solar cell*

To study the impact of the addition of CdSe BSF layer, the cell performance at different thickness and doping concentration of CdSe on CdS/CdTe/CdSe (DHJSC) has been investigated. In Fig. 5(a), the V_{OC} increases from 0.89 to 1.1 V when BSF layer thickness increases from 0 to 50 nm and shows constant up to 300 nm for the carrier concentration of 3×10^{19}–7×10^{19} cm^{-3}. As shown in Fig. 5(b), the J_{SC} gradually increases from 28.5 to 31.5 mA/cm^2 with the increase of thickness from 0 to 200 nm and then tends to be constant up to 300 nm for similar carrier concentrations. At concentration over 7×10^{19} cm^{-3}, current density decreases again with thickness might be due to the increase of carrier recombination at very high density. At carrier concentration of CdSe BSF less than 1×10^{19}, the cell current increases gradually and V_{OC} tend to be constant over 50 to 300 nm while FF start to decrease above the thickness of 200 nm. When the carrier concentration is higher than 10^{19} cm^{-3} (P^+-CdSe), the noticeable improvement of Jsc, Voc, FF and therefore the cell efficiency is observed for the CdSe thickness of > 50 nm together with smaller decrease of J_{SC}. From Fig. 5 (c) and (d), the highest efficiency of CdS/CdTe solar cell is found to be 32.6% with Voc of 1.15 V, Jsc of 32.48 mA/cm^2 and FF of 88.76% with carrier concentration of 10^{20} cm^{-3}, defect density of 10^{14} cm^{-3} for the thickness of 100 nm, beyond this thickness, very small increment of the PCE of CdS/CdTe/CdSe DHJSC is observed. At the higher carrier concentration (>5×10^{18} cm^{-3}), the CdSe BSF offers high conductive path for holes to separate as well as easily transport from CdTe absorber layer to output terminal due to existing the favorable conduction and valence band offset between absorber CdTe and CdSe BSF. The very higher carrier concentration of CdSe (>10^{20} cm^{-3}), it shows metallic behavior, conversely the diminished semiconductor behavior. Hence, the lowering of energy gradient take place, consequently electric field, that cause the small reduction of the photocurrent. When the thickness is smaller than 50 nm, the PCE is ~ 25.5% due to insignificant absorption of spectral rays in the longer wavelength. However, at the thickness of > 200, the diffusion length for holes is longer that causes the recombination of the photo-generated carriers, therefore the FF of the CdS/CdTe/CdSe cell starts to decrease. Moreover, the CdSe thickness of 100 nm with carrier

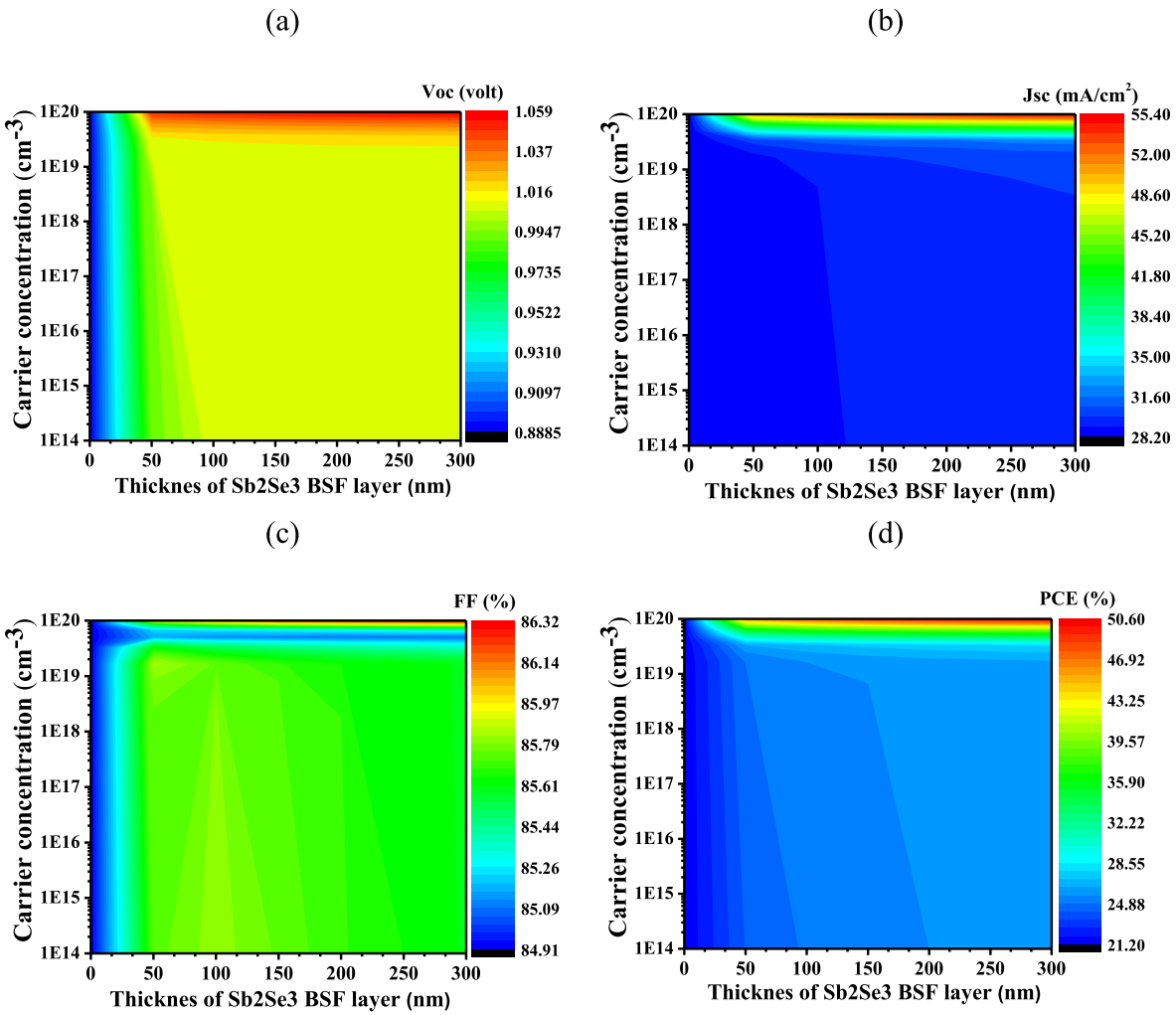

Fig. 6. The variation of output parameters (a) Voc, (b) Jsc (c) FF and (d) η of CdS/CdTe solar cells with respect to carrier concentration and thickness of Sb_2Se_3 BSF layer.

concentration of $> 10^{19}$ cm^{-3} offers best cell performance with PCE of 31.11%.

3.4. *Effect of Sb_2Se_3 BSF layer on PV performance of CdTe solar cell*

In this section, the effects of thickness and carrier concentration of Sb_2Se_3 BSF layer on photovoltaic parameters of CdS/CdTe solar cell are reported. Fig. 6 depicts the effect of thickness and carrier concentration of Sb_2Se_3 BSF layer on the PV parameters of the solar cells. The thickness and the carrier concentration of Sb_2Se_3 BSF layer are varied from 0 to 300 nm and 10^{14} to 10^{20} cm^{-3} respectively. It is visualized from Fig. 6 (a), the open circuit voltage Voc increases from 0.88 to 1.05 V with Sb_2Se_3 BSF layer and almost independent with thickness of the BSF layer from 50 to 250 nm, beyond this value the Voc tends to decrease due to the carrier recombination for enlarging the carrier's diffusion length. As seen from Fig. 6(b), the short circuit current J_{SC} is increased with increasing the carrier concentration of Sb_2Se_3 BSF layer and it is almost unchanged for the BSF layer thickness higher than 100 nm. At BSF layer thickness of $\geq$ 100 nm, the cell current is increased from 31.1 to 55.4 mA/cm^2 with increase of the carrier concentration from 10^{14} to10^{20} cm^{-3}. This drastic improvement of photocurrent due to absorption of the longer wavelength photons (as shown in Section 3.7) and therefore, creation of higher number of electron-hole pairs. The BSF Sb_2Se_3 having band gap of 1.53 eV with carrier concentration of 10^{20} cm^{-3}, shows the metal-like nature, that offers highly conductive path for hole transportation from throughout the cell to output terminal (Cai et al., 2019; Benzetta et al., 2019). It is clearly seen from Fig. 6, when carrier concentration of Sb_2Se_3 is $\sim 10^{20}$ cm^{-3} (degenerated Sb_2Se_3), even the thickness of $\sim$ 50 nm of Sb_2Se_3 BSF layer offers drastic enhancement of the cell performance to 44.14% with Jsc of 49.23 mA/cm^2, Voc of 1.05 V and FF of 85.71% keeping defect density of 10^{16} cm^{-3}, respectively. The insertion of highly degenerate Sb_2Se_3 BSF layer which produces a higher built-in potential (Hossain, J. et al., 2020) that develops higher open circuit voltage. In Fig. 6(c), the fill factor increase in very small amount (from 85.09% to 85.79) with the insertion of Sb_2Se_3 BSF layer and then retains constant with increasing the thickness at carrier concentration from 10^{14} to 10^{20} cm^{-3}. Inversely, the FF is negligible changes with increase of BSF carrier concentration from 10^{14}–10^{20} cm^{-3} at the layer thickness ranges of 50–300 nm for same carrier concentration. The photocurrent decreases from 48.6 to 44.8 mA/cm^2, consequently the PCE decreases from 44.14% to 39.6% with the increase of the defect density from 10^{12} to 10^{18} cm^{-3} whereas Voc and FF decrease small extent, this is due to the SRH recombination with increase of defect. As seen in Fig. 6 (d), the simulation results of CdS/CdTe solar cell with Sb_2Se_3 BSF reveal that the maximum efficiency reaches at 50.6% with the thickness of 100 nm, carrier concentration of $> 5x10^{19}$ cm^{-3} and defect density of 10^{16} cm^{-3}. Considering the trade-off condition among all output parameters, the optimized efficiency was found of 44.14% with Jsc of 49.23 mA/cm^2, Voc of 1.05 V and FF of 85.71%. It is notable that, these values of output parameters for CdS/CdTe based solar cell

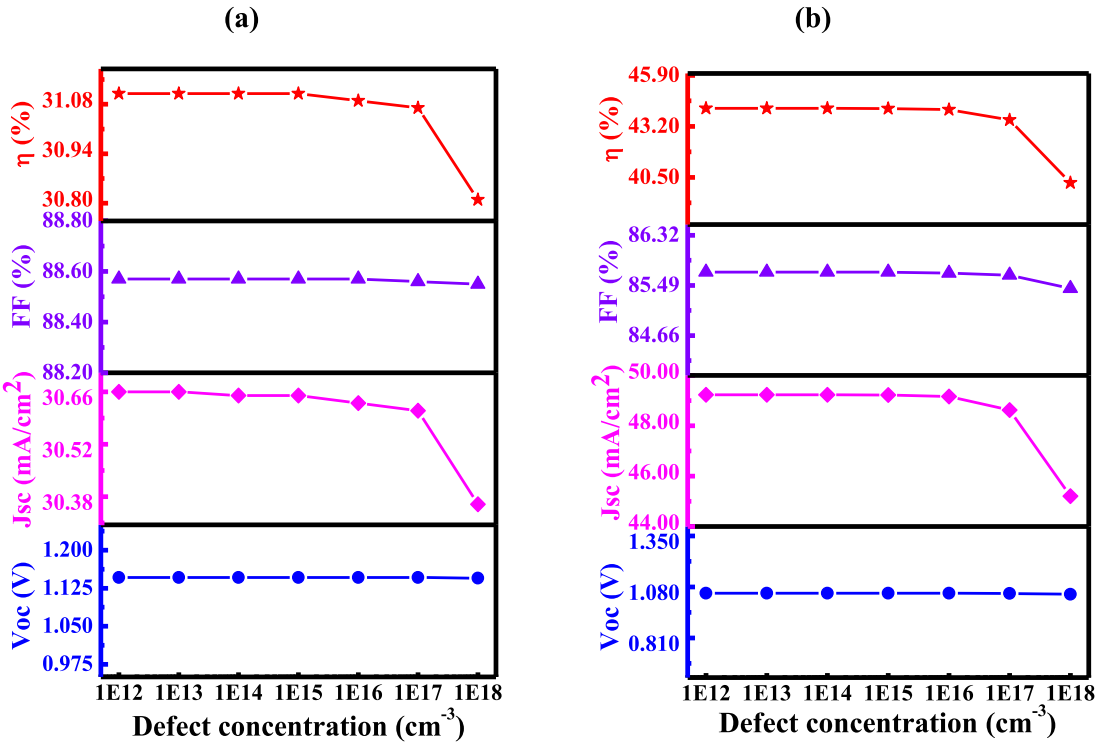

Fig. 7. The variation of output parameters (Voc, Jsc, FF and η) of CdS/CdTe/CdSe or Sb_2Se_3 DHJSC with respect to defect density of (a) CdSe and (b) Sb_2Se_3 BSF layer.

with Sb_2Se_3 BSF layer offers the highest theoretical performance to the best of our best knowledge.

3.5. *Effect of defect density of CdSe and Sb_2Se_3 on photovoltaic performance*

Fig. 7(a) shows the effect of bulk defect density of CdSe BSF layer on cell performance in the range of 10^{12}–10^{18} cm^{-3}. The photovoltaic parameters Voc, Jsc and FF are not considerably affected up to the defect density of 10^{17} cm^{-3}, above this value of the defect density ($>10^{17}$ cm^{-3}), the PCE of CdS/CdTe/CdSe DHJSC falls down slightly from ~ 31.11 to ~ 30.8% due to SRH recombination. Moreover, the optimum cell efficiency 31.11% is obtained with Voc of 1.15 V, Jsc of 30.66 mA/cm^2 and FF of 88.57% by the trade of among all the output parameters with the thickness of 100 nm, the carrier concentration of $> 10^{19}$ cm^{-3} at defect density of 10^{16} cm^{-3}, respectively. Though the improvement of PCE ~ 9% (from 21.2% to 31.1%) is much promising for CdS/CdTe based heterojunction solar cells with the addition of CdSe BSF layer, there is still opportunity to improve the cell performance as dual heterojunction solar cells the detailed-balance limit of DHSC. In such perspective, further investigations on CdS/CdTe heterostructure adding with another promising semiconducting Sb_2Se_3 as BSF layer has been carried out that offers outstanding cell performance.

Fig. 7(b) shows the bulk defect density effect in Sb_2Se_3 BSF layer on the PV performance of CdS/CdTe/Sb_2Se_3 dual heterojunction solar cell. The effect of the bulk defect density of Sb_2Se_3 is negligible up to 5×10^{16} cm^{-3} but there is noticeable impact appears for further increment beyond this value. As seen from Fig. 7(b), the photocurrent drops from 49.1 to 45.0 mA/cm^2, thus the PCE from 44.2% to 39.1% with small decrease of FF (from 85.67 to 85.1%) though Voc stand at constant value of 1.08 V. This is, since the defect causes the SRH recombination, the presence of higher density of defects have perturbed the cell output parameters, therefore the cell efficiency.

3.6. *Effect of interface defect density on photovoltaic performance*

Interface engineering one of the most crucial part of the photovoltaic technology. Fig. 8 shows solar cell performance of corresponding interface defect densities from 10^{11}–10^{17} cm^{-2} for different interface of CdS/CdTe, CdTe/CdSe and CdTe/Sb_2Se_3, respectively. Conventionally, the defect exists at the interface increase the carrier trapping probability and series resistance of the cell. The small impact of interface defect density up 10^{14} cm^{-2} is observed whereas the higher defect concentration affects the output parameters noticeably. Fig. 8(a) shows the impact of interface defect density of CdS/CdTe for the pristine CdTe solar cell i.e. the structure without any BSF layer. As seen in the Fig. 8(a), the FF decreases from 84.9% to 80.0% and the Voc decreases from 0.888 to 0.883 V, therefore the efficiency drops from 21.29% to 19.8% though the decrease of Jsc is very small from 28.22 to 28.14 mA/cm^2 with CdS/CdTe interface defect density varying from 10^{11} to 10^{17} cm^{-2}. This is due to the increase of carrier recombination rate and series resistance. The influence of CdTe/CdSe interface defect density on the cell performance of CdTe dual-heterojunction with CdSe BSF layer is depictedin Fig. 8(b). The PCE decreases from 31.11 to 26.0% with the decrease of Voc from 1.16 to 0.99 V, FF from 88.3% to 86.9% and Jsc of 30.4 to 29.5 mA/cm^2 for defect density varying from 10^{11} to 10^{17} cm^{-2} at CdTe/CdSe interface. As similar of CdS/CdTe interface, defect density below 10^{14} cm^{-2} does not noticeably but at $> 10^{14}cm^{-2}$, drops the PCE linearly. Fig. 8(c) shows the impact of defect density on output parameters for CdTe/Sb_2Se_3 interface of CdTe-DHJSC. In Fig. 8(c), the increase of defect density from 10^{11} to 10^{17} cm^{-3} at CdTe/Sb_2Se_3 interface, the V_{oc} decreases from 1.07 to 0.99 V, FF from 88.9 to 86.7% and the J_{SC} of 59.4 to 29.7 $mAcm^{-2}$, therefore the efficiency drops markedly from 55.2 to 25.2%. For the presence of high density defect at absorber/BSF interface, significant amount of photogenerated carriers are trapped and flopped to contribute to the cell performance. The higher spectral loss and carrier recombination as well as the increased of cell series resistance collectively affect the output parameters therefore the overall cell performance. This investigation on deferent interface defect density

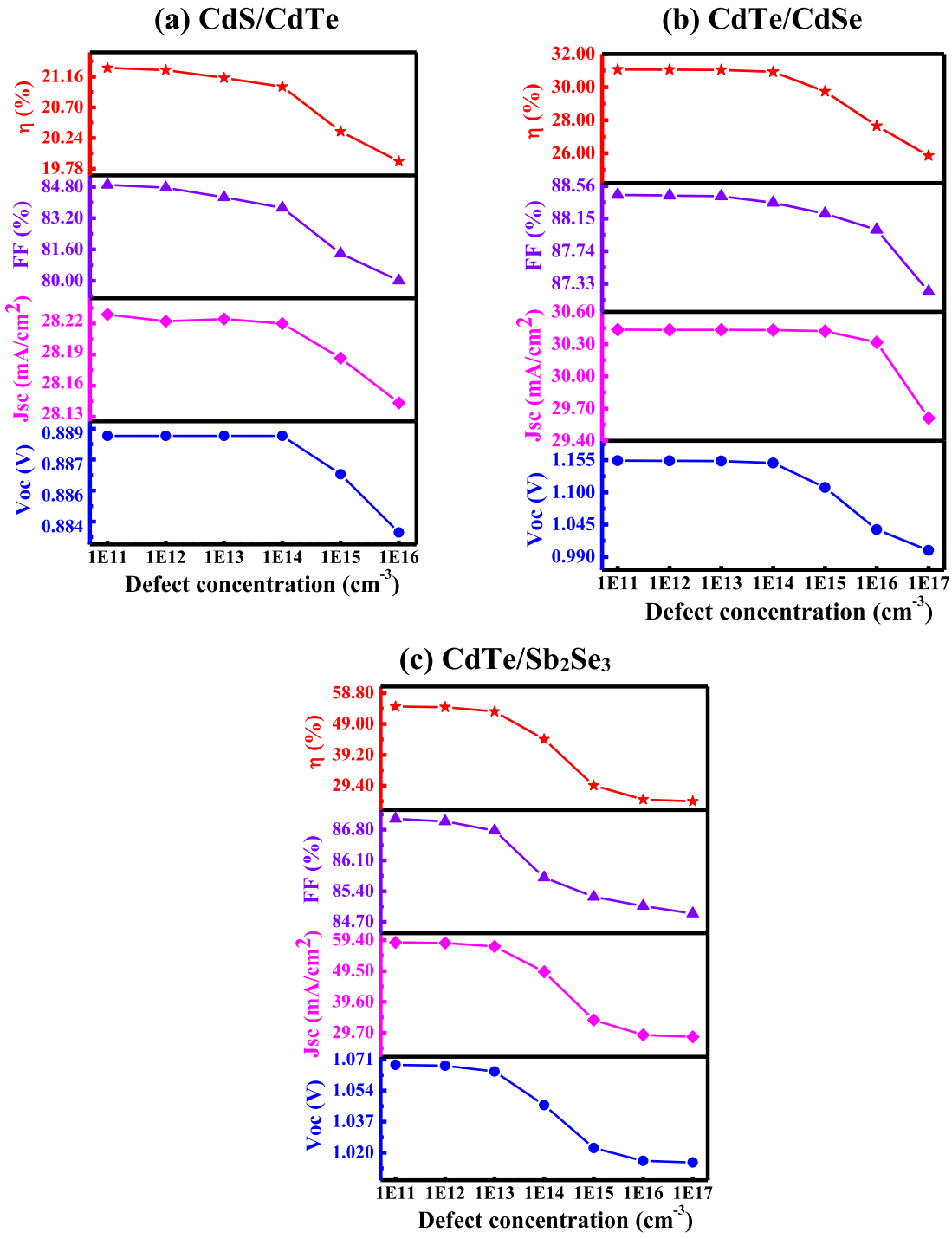

Fig. 8. The variation of output parameters (Voc, Jsc, FF and η) with respect to different interface defect: (a) CdS/CdTe interface of CdTe heterojunction solar cell and (b) CdTe/CdSe and (c) CdTe/Sb_2Se_3 interface of CdTe-based dual-heterojunction solar cells.

suggests that the interface defect density has a massive impact on the performance of the CdTe-based dual heterojunction solar cells. The interfacial defects are induced by the structural defects of the two respective materials and diffusion of metal cations through the absorber layer during cell fabrication are the key sources of the interface defect (Ahmmed et al., 2020a; Kumar and Rao, 2014). By the use of efficient technique for deposition and highly attentive concentration during fabrication of the cell, it is possible to minimize the impact of interface defect.

3.7. The effect BSF on QE of CdTe-based dual-heterojunction solar cell

Fig. 9(a) and b represent the simulated quantum efficiency (QE) of CdS/CdTe/CdSe and CdS/CdTe/Sb_2Se_3 dual-heterojunction solar cells with the variation of BSF layer thickness. It is interesting to note from the figure that QE for the solar cell is highly dependent on thickness of the both BSF layer. In Fig. 9(a), the QE of the devices increases with increasing thickness of CdSe BSF layer at the higher wavelength from 825 to 1200 nm that offers the improvement of the cell efficiency from 21.29% to 31.11%. The QE increases up to 20% corresponding the CdSe thickness retaining exponential decay in nature. On the other hand, the

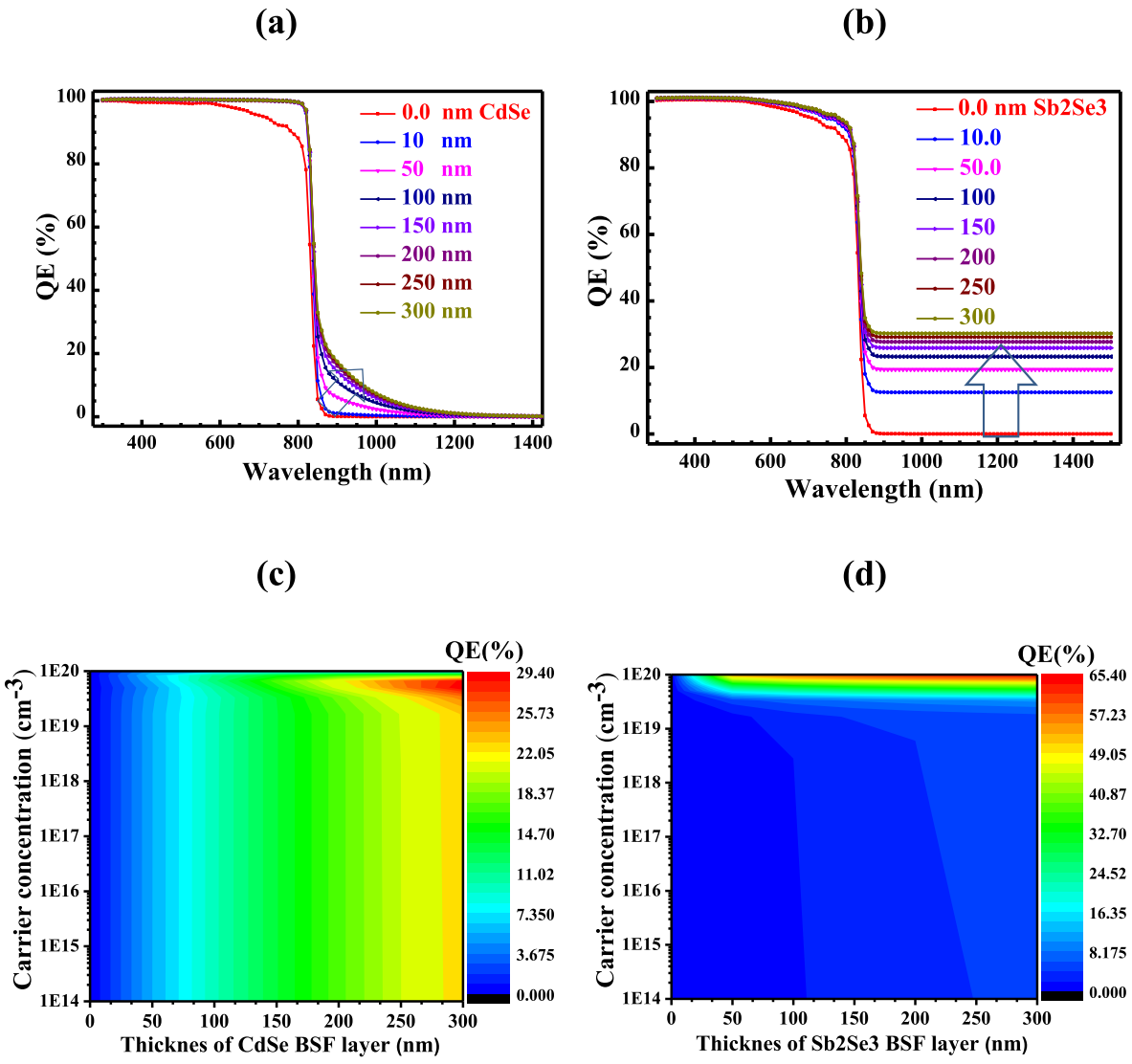

Fig. 9. The quantum efficiency (QE) of CdS/CdTe-based DHSCs at different thickness of (a) CdSe and (b) Sb_2Se_3BSF layer. And, the QE of DHSCs at constant wavelength with different concentration and thickness of (c) CdSe (at wavelength of 900 nm) and (d) Sb_2Se_3 (at wavelength of 1400 nm) BSF layer.

markedly increment of QE at the wavelength ≥ 825 nm is observed with the increase of Sb_2Se_3 BSF layer thickness from 0 to 300 nm. In this case, QE over the wavelength ≥ 825 nm is constant and it reaches up to 33% seen in Fig. 9(b). The higher absorption of the tail spectral rays offers the remarkable improvement of the cell efficiency from 21.29 to 44.14%. Fig. 9(c) and Fig. 9(d) show the improvement of QE at a specific wavelength of 900 nm and 1400 nm, respectively of CdSe and Sb_2Se_3 BSF layers at corresponding the doping concentration and thickness. The QE of the CdS/CdTe DHJSC can be improved up to 30% by the use of CdSe BSF layer at the wavelength of 900 nm whereas up to 55% for Sb_2Se_3 BSF layer at wavelength of 1400 nm with optimized carrier concentration and thickness. This may happen for two reasons: (1) the sub-band gap absorption of longer wavelength occurs in the BSF layers due to the band tail-states assisted two-step photon upconversion with the combined effect of absorption coefficient and doping density (Mondal, B.K. et al., 2021; Hossain, J., 2021; Mostaque, K., et al., 2021). As a result, the J_{SC} increases significantly despite of having higher band gap of CdSe (1.7 eV) and Sb_2Se_3 (1.53 eV) BSF layers and (2) The BSFs have much higher carrier concentration in the order of 10^{20} cm^{-3} that offers highly conductive path for photogenerated carriers to reach output terminal (Cai et al., 2019; Benzetta et al., 2019). Moreover, this type of sub-band gap absorption due to tail-states has already been reported in organic solar cells (Presselt, M., et al. 2010, Beenken, W.J.D., 2013).

3.8. *Impact of series and shunt resistances on CdTe-based dual-heterojunction solar cell*

The influences of Series (R_s) and Shunt (R_{sh}) resistance on CdTe dual-heterojunction solar cell with CdSe and Sb_2Se_3 BSF layers have been discussed in this section. These resistances are mainly originated from the contacts among the solar cell layers and metal contacts (front and back) and from the manufacturing defects (Ahmmed et al., 2020a; Mondal, B.K., et al., 2021). Fig. 10 (a) and (b) represent the impact of series and shunt resistance on cell parameters with CdSe BSF layer while Fig. 10 (c) and Fig. 10 (d), respectively represent those for Sb_2Se_3 BSF at R_s from 1 to 11 Ω-cm^2 and R_{sh} from 1.5 to 0.1 K Ω-cm^2. In Fig. 10(a), it is seen that there is no effect of series resistance on Voc and Jsc but FF is markedly affected. The FF is decreased from 87.6% to 60.3% at $R_s = 0$ to 11 Ω-cm^2 and consequently the PCE has large decrement to 19.6 from 31.29%. It is also observed from Fig. 10(b), the Voc and Jsc are constant with R_{sh} whereas the FF and therefore the efficiency are decreased from 87.5% to 58.2% and 31.29% to 21.57% respectively with the decrement of R_{sh} from 1.5 to 0.1 K Ω-cm^2. The FF and PCE are decreased drastically

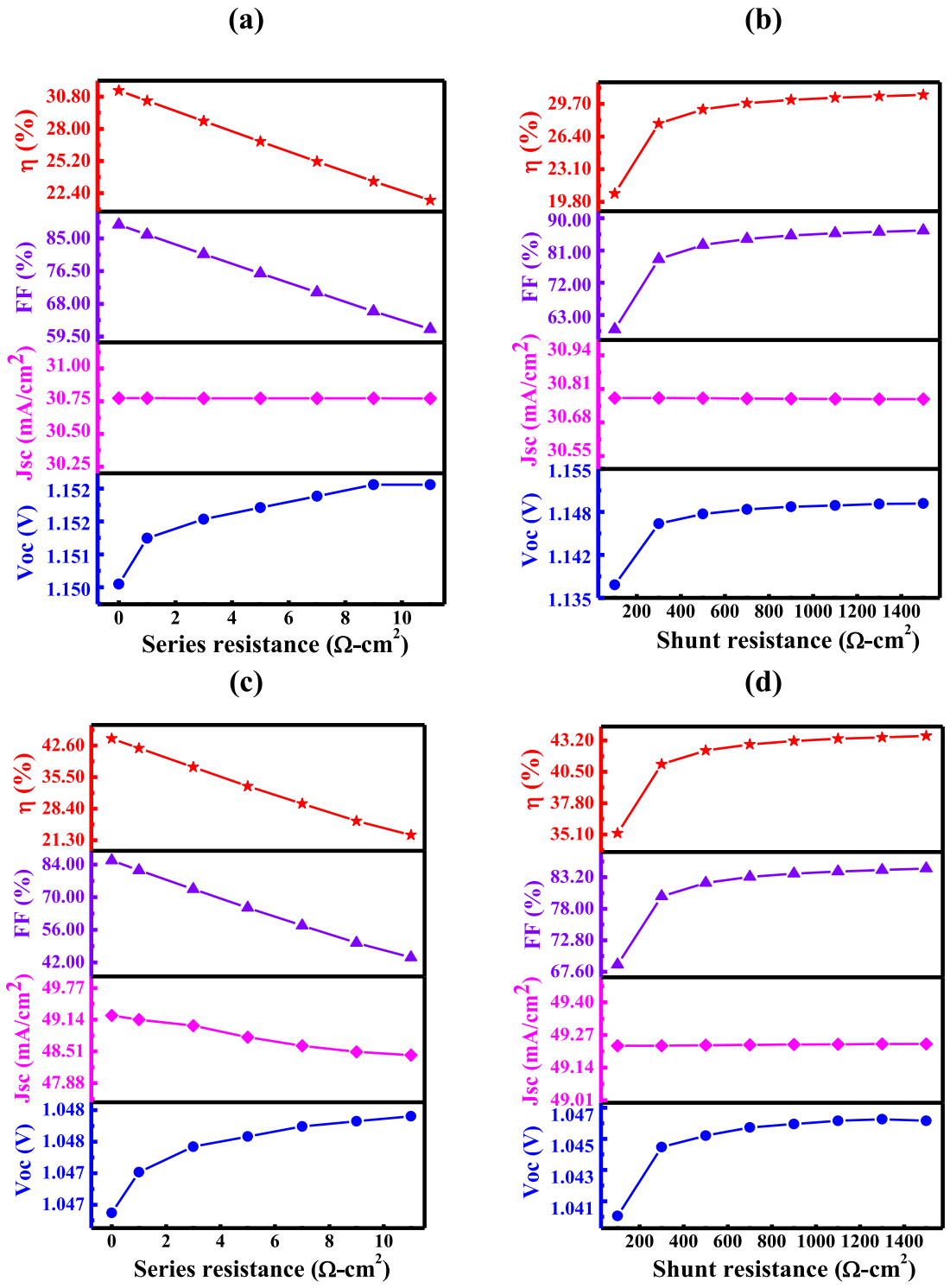

Fig. 10. The effect of series and shunt resistance of CdTe-based dual-heterojunction solar cell with (a,b) CdSe and (c,d) Sb_2Se_3 BSF layer, respectively.

from 82.3% to 58.2% and 28.5% to 21.2%, respectively with decreasing the R_{sh} from 0.5 to 0.1 K Ω-cm^2 and the output parameters are negligibly influenced when $R_{sh} \geq 0.5$ KΩ-cm^2, therefore the PCE value is retaining at ~ 31.29%.

In Fig. 10(c), it is seen that there are negligible influences of series resistance on Voc and Jsc but the FF and consequently the efficiency are decreased from 86.6% to 44.5% and 44.14% to 21.4%, respectively with increasing R_s from 1 to11 Ω-cm^2 retaining linear like nature. Also, from Fig. 10(d), the Voc and Jsc are independent with shunt resistance (R_{sh}) while the FF is decreased from 80.0% to 60.0% for the value of R_{sh} of 0.5–0.1 K Ω-cm^2 and consequently the PCE is decreased from 41.0% to 35.0% but with the R_{sh} value of ≥ 500 Ω-cm^2 they are slightly increased from 80.0% to 85.6% and 41.0% and 44.14% respectively that retains at nearly constant in nature.

3.9. *Impact of work function of back metal contact on CdS/CdTe solar cell*

Fig. 11 shows the influence of back metal contact work function (WF) on the performance of CdTe-based dual-heterojunction solar cells with

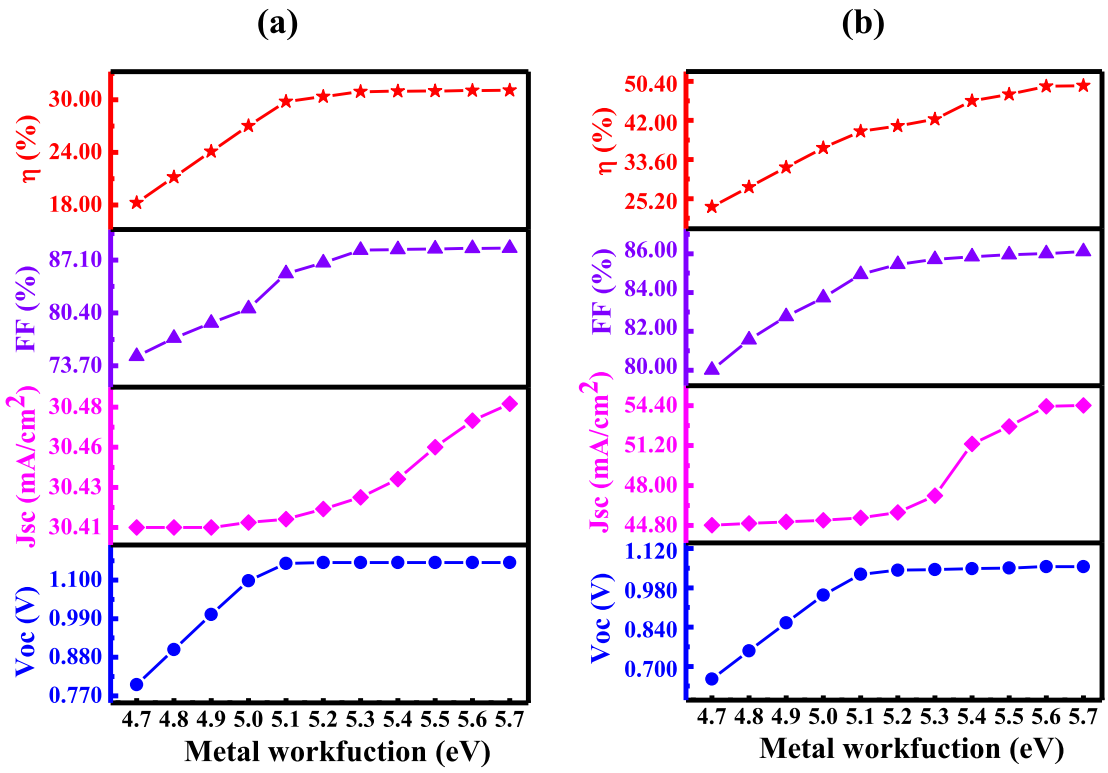

Fig. 11. The effect of back metal work function of CdTe-based dual heterojunction solar cell with (a) CdSe and (b) Sb_2Se_3 BSF layer.

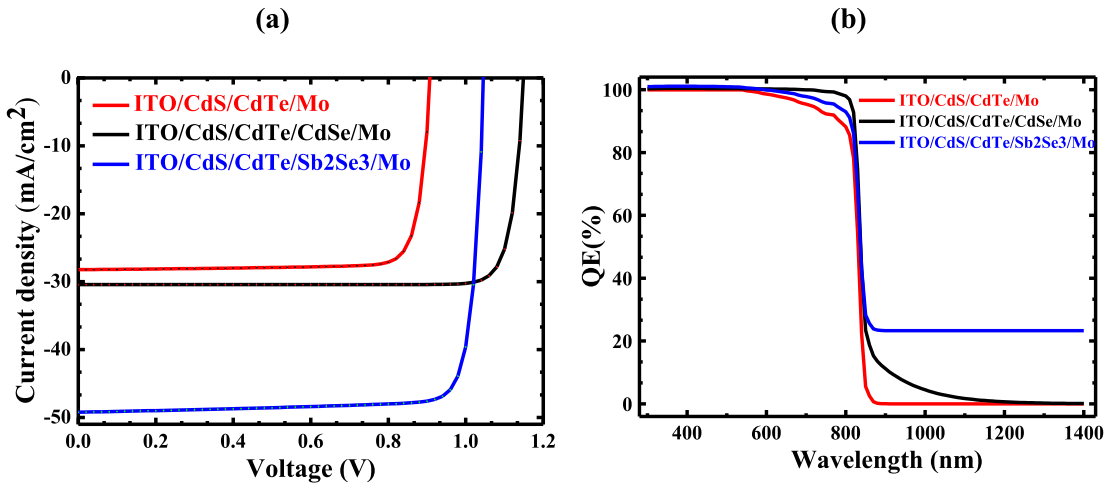

Fig. 12. (a) The J-V characteristics and (b) corresponding quantum efficiency of the CdTe-based heterojunction solar cell with and without CdSe and Sb_2Se_3 BSF layers.

the addition of CdSe or Sb_2Se_3 BSF in the range of 4.7–5.7 eV. In Fig. 11 (a), the Voc, FF and therefore the PCE increase with increasing the metal WF up to a certain WF value of ~ 5.1 eV, which indicates the decrement of barrier height with higher metal WF. The PCE saturated at WF $\geq$ 5.1 eV. A similar consequence also observed for Sb_2Se_3 BSF as seen in Fig. 11 (b). The Voc, FF and therefore the PCE increase with increasing the metal WF of Sb_2Se_3 up to a certain WF of ~ 5.4 eV, the PCE saturated at WF $\geq$ 5.4 eV due to the similar cause of lowering the barrier height and reducing the electrical loss as observed for CdSe BSF. The choice of appropriate metal contact is an essential matter to obtain the highest PCE from a heterojunction solar cell. The [1 1 0] Mo having the work function of 5.0 eV (Ranade et al., 2001) has been chosen in this study compromising between the cost and its effectiveness as back metal contact. Also, it is observed that the cell performance is gradually decreases from 31.1 to 25.8% and from 44.14 to 42.92% with working temperature WT of 300 to 400 K for CdSe and Sb_2Se_3 BSF layer respectively. The decrease of PCE 2–5% with WT indicates the degree of stability of the designed cell. An increase of temperature causes an increase in the velocity of the charge carriers and reduces the bond energy that causes decreases of band gap results in the decrease of the cell performance.

3.10. The optimized CdTe-based dual-heterojunction solar cell

The J–V characteristic and quantum efficiency (QE) of the CdS/CdTe/Mo, ITO/CdS/CdTe/CdSe/Mo and ITO/CdS/CdTe/Sb_2Se_3/Mo dual-heterojunction solar cell are depicted in Fig. 12. It is observed from Fig. 12(a), the pristine ITO/CdS/CdTe/Mo solar cell with optimized

Table 2
The optimized PV parameters for CdS/CdTe solar cell with and without BSF layer.

Device Structure	J_{SC} (mA/cm^2)	V_{OC} (v)	FF (%)	η(%)
n-CdS/CdTe	28.23	0.889	84.90	21.29
n-CdS/CdTe/p$^+$-CdSe	30.66	1.146	88.57	31.11
n-CdS/CdTe/p$^+$-Sb$_2$Se$_3$	49.23	1.046	85.71	44.14

parameters has the Voc, Jsc, FF and PCE of 0.88 V, 28.23 mA/cm^2, 84.95% and 21.29% respectively. On other hand, the optimized ITO/CdS/CdTe/CdSe/Mo heterostructure achieved the PCE of 31.11% with Voc of 1.15 V, Jsc of 30.66 mA/cm^2 and FF of 88.57%, respectively. Whereas the Voc, Jsc, FF and PCE of 1.05 V, 49.23 mA/cm^2, 85.71% and 44.14%, respectively are achieved from the optimized ITO/CdS/CdTe/Sb_2Se_3/Mo heterostructure The addition of CdSe and Sb_2Se_3 offer the massive enhancement of PCE of ~ 10 and ~ 23% respectively as shown in Fig. 12(a). As observed in Fig. 12(b), the quantum efficiency of the designed CdTe-based dual-heterojunction solar cells improved at wavelength, $\lambda > 800$ nm after the incorporation of CdSe and Sb_2Se_3 BSF layer. The insertion of Sb_2Se_3 BSF, a drastic improvement of absorption at higher wavelength ($\lambda > 800$) is appeared that provides origin of the huge improvement of cell performance. Table 2 represents the summary of the optimized PV parameters of CdTe-based dual-heterojunction solar cells with and CdSe and Sb_2Se_3 BSF layers.

4. Conclusions

The performance of the highly efficient CdTe-based dual-heterojunction solar cells with CdSe and Sb_2Se_3 BSF layers have been studied using SCAPS-1D simulator. The simulation results refer that the insertion of CdSe and Sb_2Se_3 as BSF significantly improves the output parameters, therefore the performance of the solar cells. The optimized PCE of the pristine CdS/CdTe solar cell without any BSF layer is about 21.29%. Where, the addition of CdSe BSF layer offers the PCE of the solar cell of 31.11% with enhanced Voc of 1.15 V, Jsc of 30.66 mA/cm^2 and FF of 88.57%, respectively. On the other hand, the addition of Sb_2Se_3 BSF layer the drastically enhanced the PCE of the solar cell to 44.14% with the Voc of 1.05 V, Jsc of 49.23 mA/cm^2 and the FF of 85.71%, respectively. Increased absorption of the longer wavelength light in the BSF due to tail-states assisted upconversion offers such a drastic improvement of the DHJSC with suitable BSF layers. These entire theoretical analyses reveal that the CdSe and Sb_2Se_3 BSF layers, those can be deposited by low cost methods, pose huge potentiality for practical fabrication of high performance CdTe-based dual- heterojunction solar cells for harnessing the solar energy.

Declaration of Competing Interest

The authors declare that they have no known competing financial interests or personal relationships that could have appeared to influence the work reported in this paper.

Acknowledgements

The authors highly appreciate Dr. Marc Burgelman, University of Gent, Belgium, for providing SCAPS simulation software.

References

Absorption Coefficient | PVEducation [WWW Document], n.d. URL https://www.pveducation.org/pvcdrom/pn-junctions/absorption-coefficient (accessed 4.8.21).

Ahmmed, S., Aktar, A., Hossain, J., Ismail, A.B.M., 2020a. Enhancing the open circuit voltage of the SnS based heterojunction solar cell using NiO HTL. Sol. Energy 207, 693–702. https://doi.org/10.1016/j.solener.2020.07.003.

Ahmmed, S., Aktar, A., Rahman, M.F., Hossain, J., Ismail, A.B.M., 2020b. A numerical simulation of high efficiency CdS/CdTe based solar cell using NiO HTL and ZnO TCO. Optik (Stuttg). 223, 165625. https://doi.org/10.1016/j.ijleo.2020.165625.

Moon, M.M.A., Rahman, M.F., Kamruzzaman, M.d., Hossain, J., Ismail, A.B.M., 2021. Unveiling the prospect of a novel chemical route for synthesizing solution- processed CdS / CdTe thin-film solar cells Unveiling the prospect of a novel chemical route for synthesizing solution-processed CdS / CdTe thin-film solar cells. Energy Rep. 7, 1742–1756. https://doi.org/10.1016/j.egyr.2021.03.031.

Andreani, L.C., Bozzola, A., Kowalczewski, P., Liscidini, M., Redorici, L., 2019. Silicon solar cells: Toward the efficiency limits. Adv. Phys. X 4 (1), 1548305. https://doi.org/10.1080/23746149.2018.1548305.

Baines, T., Zoppi, G., Bowen, L., Shalvey, T.P., Mariotti, S., Durose, K., Major, J.D., 2018. Incorporation of CdSe layers into CdTe thin film solar cells. Sol. Energy Mater. Sol. Cells 180, 196–204. https://doi.org/10.1016/j.solmat.2018.03.010.

Bao, Z., Yang, X., Li, B., Luo, R., Liu, B.o., Tang, P., Zhang, J., Wu, L., Li, W., Feng, L., 2016. The study of CdSe thin film prepared by pulsed laser deposition for CdSe/CdTe solar cell. J. Mater. Sci. Mater. Electron. 27 (7), 7233–7239. https://doi.org/10.1007/s10854-016-4689-9.

Battaglia, C., Cuevas, A., De Wolf, S., 2016. High-efficiency crystalline silicon solar cells: Status and perspectives. Energy Environ. Sci. 9 (5), 1552–1576. https://doi.org/10.1039/C5EE03380B.

Bayramoglu, H., Peksöz, A., Easy production of p-type cdse absorber layer by co-electrodeposition. Turkish physical society 33rd international physics congress, september 6-10, 2017, bodrum /turkey.

Beenken, W.J.D., Herrmann, F., Presselt, M., Hoppe, H., Shokhovets, S., Gobsch, G., Runge, E., 2013. Sub-bandgap absorption in organic solar cells: Experiment and theory. Phys. Chem. Chem. Phys. 15, 16494–16502. https://doi.org/10.1039/c3cp42236d.

Benzetta, A.E.H., Abderrezek, M., Djeghlal, M.E., 2019. Contribution to improve the performances of Cu2ZnSnS4 thin-film solar cell via a back surface field layer. Optik (Stuttg). 181, 220–230. https://doi.org/10.1016/j.ijleo.2018.12.048.

Bhattacharya, S., John, S., 2019. Beyond 30 % conversion efficiency in silicon solar cells : a numerical demonstration. Sci. Rep. 1–15 https://doi.org/10.1038/s41598-019-48981-w.

Biplab, S.R.I., Ali, M.H., Moon, M.M.A., Pervez, M.F., Rahman, M.F., Hossain, J., 2020. Performance enhancement of CIGS-based solar cells by incorporating an ultrathin BaSi2 BSF layer. J. Comput. Electron. 19 (1), 342–352. https://doi.org/10.1007/s10825-019-01433-0.

Birkett, M., Linhart, W.M., Stoner, J., Phillips, L.J., Durose, K., Alaria, J., Major, J.D., Kudrawiec, R., Veal, T.D., 2018. Band gap temperature-dependence of close-space sublimation grown Sb2Se3 by photo-reflectance. APL Mater. 6 (8), 084901. https://doi.org/10.1063/1.5027157.

Burgelman, M., Verschraegen, J., Degrave, S., Nollet, P., 2004. Modeling thin-film PV devices. Prog. Photovoltaics Res. Appl. 12 (23), 143–153. https://doi.org/10.1002/(ISSN)1099-159X10.1002/pip.v12:2/310.1002/pip.524.

Burst, J.M., Duenow, J.N., Albin, D.S., Colegrove, E., Reese, M.O., Aguiar, J.A., Jiang, C. S., Patel, M.K., Al-Jassim, M.M., Kuciauskas, D., Swain, S., Ablekim, T., Lynn, K.G., Metzger, W.K., 2016. CdTe solar cells with open-circuit voltage breaking the 1V barrier. Nat. Energy 1. https://doi.org/10.1038/NENERGY.2016.15.

Cai, L., Wang, W., Jin, L., Yao, Z., Lin, W., Meng, L., Ai, B., Liang, Z., Huang, Y., Zhang, F., Altermatt, P.P., Shen, H., 2019. 12.29% low temperature-processed dopant-free CdS/p-Si heterojunction solar cells. Adv. Mater. Interfaces 6 (12), 1900367. https://doi.org/10.1002/admi.v6.1210.1002/admi.201900367.

Černošková, E., Todorov, R., Černošek, Z., Holubová, J., Beneš, L., 2014. Thermal properties and the structure of amorphous Sb 2 Se 3 thin film. J. Therm. Anal. Calorim. 118 (1), 105–110. https://doi.org/10.1007/s10973-014-4000-3.

Chate, P.A., Patil, S.S., Patil, J.S., Sathe, D.J., Hankare, P.P., 2012. Nanocrystalline CdSe: Structural and photoelectrochemical characterization. Electron. Mater. Lett. 8 (6), 553–558. https://doi.org/10.1007/s13391-012-2069-z.

Chen, C., Li, W., Zhou, Y., Chen, C., Luo, M., Liu, X., Zeng, K., Yang, B.o., Zhang, C., Han, J., Tang, J., 2015. Optical properties of amorphous and polycrystalline Sb2Se3 thin films prepared by thermal evaporation. Appl. Phys. Lett. 107 (4), 043905. https://doi.org/10.1063/1.4927741.

Chen, S., Qiao, X., Zheng, Z., Cathelinaud, M., Ma, H., Fan, X., Zhang, X., 2018. Enhanced electrical conductivity and photoconductive properties of Sn-doped Sb2Se3 crystals. J. Mater. Chem. C 6 (24), 6465–6470. https://doi.org/10.1039/C8TC01683F.

De Vos, A., 1980. Detailed balance limit of the efficiency of tandem solar cells. J. Phys. D. Appl. Phys. 13, 839–846. https://doi.org/10.1088/0022-3727/13/5/018.

Dimroth, F., Grave, M., Beutel, P., Fiedeler, U., Karcher, C., Tibbits, T.N.D., Oliva, E., Siefer, G., Schachtner, M., Wekkeli, A., Bett, A.W., Krause, R., Piccin, M., Blanc, N., Drazek, C., Guiot, E., Ghyselen, B., Salvetat, T., Tauzin, A., Signamarcheix, T., Dobrich, A., Hannappel, T., Schwarzburg, K., 2014. Wafer bonded four-junction GaInP/GaAs//GaInAsP/GaInAs concentrator solar cells with 44.7% efficiency. Prog. Photovoltaics Res. Appl. 22 (3), 277–282. https://doi.org/10.1002/pip.v22.310.1002/pip.2475.

El-Sayad, E.A., 2008. Compositional dependence of the optical properties of amorphous Sb2Se3-xSx thin films. J. Non. Cryst. Solids 354 (32), 3806–3811. https://doi.org/10.1016/j.jnoncrysol.2008.05.004.

El-Shair, H.T., Ibrahim, A.M., Abd El-Wahabb, E., Afify, M.A., Abd El-Salam, F., 1991. Optical properties of Sb2Se3 thin films. Vacuum 42 (14), 911–914. https://doi.org/10.1016/0042-207X(91)90557-Y.

Enkhardt, S., 2020. CIGS cells could hit efficiencies of 33%, say Germany scientists. pv magazine International. https://www.pv-magazine.com/2020/10/09/cigs-cells-could-hit-efficiencies-of-33-say-germany-scientists/ (accessed 4.3.21).

Gao, X., Luo, W., Zhang, Y., Hu, R., Zhang, B., Züttel, A., 2020. Stable and High-Efficiency Methylammonium-Free Perovskite Solar Cells 1905502, 1–9. https://doi.org/10.1002/adma.201905502.

Green, M.A., 2001. Third generation photovoltaics: Ultra-high conversion efficiency at low cost. Prog. Photovoltaics Res. Appl. 9 (2), 123–135. https://doi.org/10.1002/(ISSN)1099-159X10.1002/pip.v9:210.1002/pip.360.

Green, M.A., Dunlop, E.D., Hohl-Ebinger, J., Yoshita, M., Kopidakis, N., Hao, X., 2020. Solar cell efficiency tables (version 56). Prog. Photovoltaics Res. Appl. 28 (7), 629–638. https://doi.org/10.1002/pip.v28.710.1002/pip.3303.

Henry, C.H., Nassau, K., Shiever, J.W., 1971. Optical studies of shallow acceptors in CdS and CdSe. Phys. Rev. B 4 (8), 2453–2463. https://doi.org/10.1103/PhysRevB.4.2453.

Hu, X., Wang, H., Ying, Y., Wang, M., Zhang, C., Ding, Y., Li, H., Li, W., Zhao, S., Zang, Z., 2020. Methylammonium chloride as an interface modificator for planar-structure perovskite solar cells with a high open circuit voltage of 1.19V. J. Power Sources 480, 229073. https://doi.org/10.1016/j.jpowsour.2020.229073.

Hossain, J., Islam, A.T.M.S., Kasahara, K., Ishikawa, R., Ueno, K., Shira, H., 2021. State-of-the-art of solution-processed crystalline silicon/organic heterojunction solar cells: Challenges and future, in Development of Solar Cells- Theory and Experiment, (Accepted). Springer International Publishing, Springer Nature Switzerland AG.

Hossain, J., Moon, M.M.A., Mondal, B.K., Halim, M.A., 2020. Design guidelines for a highly efficient high-purity Germanium (HPGe)-based double-heterojunction solar cell. arXiv Prepr. 1–23. arXiv:2009.13948 [physics.app-ph].

Khudiar, A.I., Khan, Z.H., Zulfequar, M., 2012. Laser-induced Effects: on Metal Chalcogenide Thin Films. LAP LAMBERT Academic Publishing. https://www.researchgate.net/publication/236068782.

Kosek, F., Tulka, J., Štourač, L., 1978. Optical, photoelectric and electric properties of single-crystalline Sb2Se3. Czechoslov. J. Phys. 28 (3), 325–330. https://doi.org/10.1007/BF01597220.

Kuddus, A., Rahman, M.F., Ahmmed, S., Hossain, J., Ismail, A.B.M., 2019. Role of facile synthesized V2O5 as hole transport layer for CdS/CdTe heterojunction solar cell: Validation of simulation using experimental data. Superlattices Microstruct. 132, 106168. https://doi.org/10.1016/j.spmi.2019.106168.

Kuddus, A., Rahman, M.F., Hossain, J., Bakar Md Ismail, A., 2020. Enhancement the Performance of CdS/CdTe Heterojunction Solar Cell Using TiO2/ZnO Bi-layer ARC and V2O5 BSF layers: A Simulation Approach. Eur. Phys. J. Appl. Phys. 20901. https://doi.org/10.1051/epjap/2020200213.

Kumar, S. Girish, Rao, K.S.R. Koteswara, 2014. Physics and chemistry of CdTe/CdS thin film heterojunction photovoltaic devices: Fundamental and critical aspects. Energy Environ. Sci. 7 (1), 45–102. https://doi.org/10.1039/C3EE41981A.

Lakshmi Shree, B., Selva Priya, S., Therasa Ranjani, P., Karthick, P., Jeyadheepan, K., Sridharan, M., 2016. Influence of CdTe thickness on the properties of vacuum evaporated CdSe/CdTe bilayer. Mater. Today Proc. 3 (6), 1494–1501. https://doi.org/10.1016/j.matpr.2016.04.033.

Li, C., Wang, F., Chen, Y., Wu, L., Zhang, J., Li, W., He, X., Li, B., Feng, L., 2018. Characterization of sputtered CdSe thin films as the window layer for CdTe solar cells. Mater. Sci. Semicond. Process. 83, 89–95. https://doi.org/10.1016/j.mssp.2018.04.022.

Li, Z., Liang, X., Li, G., Liu, H., Zhang, H., Guo, J., Chen, J., Shen, K., San, X., Yu, W., Schropp, R.E.I., Mai, Y., 2019a. 9.2%-Efficient core-shell structured antimony selenide nanorod array solar cells. Nat. Commun. 10, 1–9. https://doi.org/10.1038/s41467-018-07903-6.

Li, Zhen-Qi, Ni, Ming, Feng, Xiao-Dong, 2019b. Simulation of the Sb2Se3 solar cell with a hole transport layer. Mater. Res. Express 7 (1), 016416. https://doi.org/10.1088/2053-1591/ab5fa7.

Liu, Chunmin, Yuan, Yafei, Cheng, Ling, Su, Jing, Zhang, Xingtong, Li, Xiangxiang, Zhang, Hao, Xu, Min, Li, Jing, 2019. A study on optical properties of Sb_2Se_3 thin films and resistive switching behavior in Ag/Sb_2Se_3/W heterojunctions. Results Phys. 13, 102228. https://doi.org/10.1016/j.rinp.2019.102228.

Mondal, Bipanko Kumar, Mostaque, Shaikh Khaled, Rashid, Md. Abdur, Kuddus, Abdul, Shirai, Hajime, Hossain, Jaker, 2021. Effect of CdS and In_3Se_4 BSF layers on the photovoltaic performance of PEDOT:PSS/n-Si solar cells: Simulation based on experimental data. Superlattices Microstruct. 152, 106853. https://doi.org/10.1016/j.spmi.2021.106853.

Moon, Md. Mahabub Alam, Ali, Md. Hasan, Rahman, Md. Ferdous, Hossain, Jaker, Ismail, Abu Bakar Md., 2020. Design and simulation of $FeSi_2$-based novel heterojunction solar cells for harnessing visible and near-infrared light. Phys. Status Solidi Appl. Mater. Sci. 217 (6), 1900921. https://doi.org/10.1002/pssa:v217.610.1002/pssa:201900921.

Mostaque, S.K., Mondal, B.K., Hossain, J., 2021. Simulation approach to reach the SQ limit in CIGS-based dual-heterojunction solar cell. arXiv:2103.08841 [physics.app-ph].

Movla, Hossein, 2014. Optimization of the CIGS based thin film solar cells: Numerical simulation and analysis. Optik (Stuttg). 125 (1), 67–70. https://doi.org/10.1016/j.ijleo.2013.06.034.

Mueller, R., Wood, C., 1972. The preparation of amorphous thin films. J. Non. Cryst. Solids 7 (4), 301–308. https://doi.org/10.1016/0022-3093(72)90266-9.

Munshi, A.H., Kephart, J.M., Abbas, A., Shimpi, T.M., Barth, K.L., Walls, J.M., Sampath, W.S., 2018. Polycrystalline CdTe photovoltaics with efficiency over 18% through improved absorber passivation and current collection. Sol. Energy Mater. Sol. Cells 176, 9–18. https://doi.org/10.1016/j.solmat.2017.11.031.

Ohtsuka, Takeo, Kawamata, Junji, Zhu, Ziqiang, Yao, Takafumi, 1994. P-type CdSe grown by molecular beam epitaxy using a nitrogen plasma source. Appl. Phys. Lett. 65 (4), 466–468. https://doi.org/10.1063/1.112338.

Parashar, Devanshi, Krishna, V. S. Ganesha, Moger, Sahana Nagappa, Keshav, Rashmitha, Mahesha, M.G., 2020. Thickness optimization of ZnO/CdS/CdTe solar cell by numerical simulation. Trans. Electr. Electron. Mater. 21 (6), 587–593. https://doi.org/10.1007/s42341-020-00209-9.

Paudel, Naba R., Yan, Yanfa, 2014. Enhancing the photo-currents of CdTe thin-film solar cells in both short and long wavelength regions. Appl. Phys. Lett. 105 (18), 183510. https://doi.org/10.1063/1.4901532.

Presselt, M., Bärenklau, M., Rösch, R., Beenken, W.J.D., Runge, E., Shokhovets, S., Hoppe, H., Gobsch, G., 2010. Subbandgap absorption in polymer-fullerene solar cells. Appl. Phys. Lett. 97 (25), 253302. https://doi.org/10.1063/1.3527077.

Clover, I., PV Magazine, First Solar Raises Bar for CdTe with 21.5% Efficiency Record, 6 February 2015. http://www.https://www.pv-magazine.com/2015/02/06/first-solar-raises-bar-for-cdte-with-21-5-efficiency-record_100018069, 2015 (access, 15.11. 2020).

Rahman, Md. Ferdous, Hossain, Jaker, Kuddus, Abdul, Tabassum, Samia, Rubel, Mirza H. K., Rahman, Md. Mahbubor, Moriya, Yuma, Shirai, Hajime, Ismail, Abu Bakar Md., 2020a. A novel CdTe ink-assisted direct synthesis of CdTe thin films for the solution-processed CdTe solar cells. J. Mater. Sci. 55 (18), 7715–7730. https://doi.org/10.1007/s10853-020-04578-7.

Rahman, M.F., Hossain, J., Kuddus, A., Tabassum, S., Rubel, M.H.K., Shirai, H., Ismail, A. B.M., 2020b. A novel synthesis and characterization of transparent CdS thin films for CdTe/CdS solar cells. Appl. Phys. A Mater. Sci. Process. 126, 1–11. https://doi.org/10.1007/s00339-020-3331-0.

Ranade, P., Takeuchi, H., King, T.J., Hu, C., 2001. Work function engineering of molybdenum gate electrodes by nitrogen implantation. Electrochem. Solid-State Lett. 4, 85–87. https://doi.org/10.1149/1.1402497.

Razykov, T.M., Ferekides, C.S., Morel, D., Stefanakos, E., Ullal, H.S., Upadhyaya, H.M., 2011. Solar photovoltaic electricity: Current status and future prospects. Sol. Energy 85 (8), 1580–1608. https://doi.org/10.1016/j.solener.2010.12.002.

Ren, Donglou, Chen, Shuo, Cathelinaud, Michel, Liang, Guangxing, Ma, Hongli, Zhang, Xianghua, 2020. Fundamental physical characterization of Sb2Se3-based quasi-homojunction thin film solar cells. ACS Appl. Mater. Interfaces 12 (27), 30572–30583. https://doi.org/10.1021/acsami.0c0818010.1021/acsami.0c08180.s001.

Najim, S.A., Jamil, N.Y., 2018. The Effect of Al Doping on Structural, Electrical and Optical Properties of CdSe Films. College of Science/ University of Mosul, College of Science/ University of Mosul https://doi.org/10.33899/rjs.2018.145400.

Shenouda, Atef Y., El Sayed, El Sayed M., 2015. Electrodeposition, characterization and photo electrochemical properties of CdSe and CdTe. Ain Shams Eng. J. 6 (1), 341–346. https://doi.org/10.1016/j.asej.2014.07.010.

Simya, O.K., Mahaboobbatcha, A., Balachander, K., 2015. A comparative study on the performance of Kesterite based thin film solar cells using SCAPS simulation program. Superlattices Microstruct. 82, 248–261. https://doi.org/10.1016/j.spmi.2015.02.020.

Suzuki, Hiromichi, 1966. Electron affinity of semiconducting compound CdSe. Jpn. J. Appl. Phys. 5 (12), 1253–1254. https://doi.org/10.1143/JJAP.5.1253.

Tinedert, I.E., Pezzimenti, F., Megherbi, M.L., Saadoune, A., 2020. Design and simulation of a high efficiency CdS/CdTe solar cell. Optik (Stuttg). 208, 164112. https://doi.org/10.1016/j.ijleo.2019.164112.

Wang, Huaxin, Cao, Siliang, Yang, Bo, Li, Haiyun, Wang, Ming, Hu, Xiaofei, Sun, Kuan, Zang, Zhigang, 2020a. NH4Cl-modified ZnO for high-performance CsPbIBr 2 perovskite solar cells via low-temperature process. Sol. RRL 4 (1), 1900363. https://doi.org/10.1002/solr.v4.110.1002/solr.201900363.

Wang, Huaxin, Li, Haiyun, Cao, Siliang, Wang, Ming, Chen, Jiangzhao, Zang, Zhigang, 2020b. Interface modulator of ultrathin magnesium oxide for low-temperature-processed inorganic CsPbIBr 2 perovskite solar cells with efficiency over 11%. Sol. RRL 4 (9), 2000226. https://doi.org/10.1002/solr.v4.910.1002/solr.202000226.

Wang, Ming, Li, Wei, Wang, Huaxin, Yang, Ke, Hu, Xiaofei, Sun, Kuan, Lu, Shirong, Zang, Zhigang, 2020c. Small molecule modulator at the interface for efficient perovskite solar cells with high short-circuit current density and hysteresis free. Adv. Electron. Mater. 6 (10), 2000604. https://doi.org/10.1002/aelm.v6.1010.1002/aelm.202000604.

Yadav, A.A., Barote, M.A., Masumdar, E.U., 2010. Photoelectrochemical properties of spray deposited n-CdSe thin films. Sol. Energy 84 (5), 763–770. https://doi.org/10.1016/j.solener.2010.01.026.

Yang, X., Liu, B., Li, B., Zhang, J., Li, W., Wu, L., Feng, L., 2016. Preparation and characterization of pulsed laser deposited a novel CdS/CdSe composite window layer for CdTe thin film solar cell. Appl. Surf. Sci. 367, 480–484. https://doi.org/10.1016/j.apsusc.2016.01.224.

Yoshikawa, Kunta, Kawasaki, Hayato, Yoshida, Wataru, Irie, Toru, Konishi, Katsunori, Nakano, Kunihiro, Uto, Toshihiko, Adachi, Daisuke, Kanematsu, Masanori, Uzu, Hisashi, Yamamoto, Kenji, 2017. Silicon heterojunction solar cell with interdigitated back contacts for a photoconversion efficiency over 26%. Nat. Energy 2 (5). https://doi.org/10.1038/nenergy.2017.32.

Zhang, C., Zhang, J., Ma, X., Feng, Q., Zhang, C., Zhang, J., Ma, X., Feng, Q., 2021. CdTe Solar Cells, in: Semiconductor Photovoltaic Cells. Springer Singapore, pp. 293–324. https://doi.org/10.1007/978-981-15-9480-9_7.